

On the Spatial Distribution of Hard X-Rays from Solar Flare Loops

Vahé Petrosian¹ and Timothy Q. Donaghy²

Center for Space Science and Astrophysics

Stanford University

Stanford, CA 94305-4060

Received _____; accepted _____

¹Also Department of Physics and Applied Physics

²Also Department of Physics

ABSTRACT

The aim of this paper is to investigate the spatial structure of the impulsive phase hard X-ray emission from solar flares. This work is motivated by the YOHKOH and the forthcoming HESSI observations. Summarizing past results, it is shown that the transport effects can account for the observations by inhomogeneous loops where there is a strong field convergence and/or density enhancement at the top of the flaring loop. Scattering by plasma turbulence at the acceleration site or pancake type pitch angle distribution of the accelerated electrons can also give rise to enhanced emission at the loop tops. These could be a natural consequence of acceleration by plasma waves. This paper considers a general case of stochastic scattering and acceleration that leads to an isotropic pitch angle distribution and an enhanced emission from the loop tops or the acceleration site.

Following the formalism developed in earlier papers the strength and the spectrum of the radiation expected from the acceleration site and the foot points are evaluated and their dependence on the parameters describing the acceleration process and the flare plasma are determined. The theoretical ratio of these two intensities and relative values of their spectral indices are compared with the YOHKOH observations, demonstrating that the above mentioned parameters can be constrained with such observations. It is shown that future high spatial and spectral resolution observations, for example those expected from HESSI, can begin to distinguish between different models and constrain their parameters.

Subject Headings: acceleration of particles–plasmas–waves–Sun:flares–Sun:X-rays, gamma rays

1. Introduction

It is well established that electrons and protons are accelerated to relativistic energies during the impulsive phase of solar flares. However, the source of energy and the acceleration mechanism are not well understood. In the standard thick target model, it is assumed that the acceleration arises in the reconnection region somewhere above a flaring loop. Unfortunately, these loops are observed and delineated not by the direct radiation from the accelerated particles (hard X-rays, gamma-rays and microwave radiation) but by the thermal emissions (soft X-rays, optical, etc.) from plasmas heated and evaporated by the dissipation in the lower corona and the chromosphere of the energy of the accelerated particles. High spatial resolution observations of the direct radiation to fully map the flares during the impulsive phase are more difficult. Nonetheless, there exist some concrete results which, for the most part, agree with the above picture.

There have been several high spatial resolution observations at the microwave region by OVRO, VLA and BIMA radio telescopes. However, interpretation of the spatial distribution of the microwave emissions is complicated by the fact that it depends not only on the characteristics of the accelerated electrons, but also strongly on the strength and geometry of the magnetic field. In the case of symmetric loops, the appearance of circularly polarized radiation from the loops (Marsh & Hurford, 1980) agrees with the standard model of accelerated electrons injected at the top of the loop (Petrosian, 1982). More recent observations have revealed foot point emission primarily from one end of the loop, indicating the presence of strong asymmetry such that most of the radiation arises from the foot point with the higher magnetic field, emphasizing the dependence on the field strength and its variations. We shall not deal with microwave radiation in this paper.

Here we are concerned with the spatially resolved hard X-ray observations. First resolved images of hard X-ray impulsive emissions were provided by the SMM and

HINOTORI space crafts, showing that in majority of flares most of the emission arises from two foot point regions as expected in the standard thick target model. A more reliable confirmation of this picture has come from the YOHKOH satellite, which has detected impulsive hard X-ray emission from an area near the top of the loop, as well as the foot points, from several flares (Masuda et al. 1995). In general, this loop top emission is weaker and is more readily detectable in limb flares. Masuda (1994) finds loop top emission in six of ten such flares, indicating that this characteristic is common and may be the rule rather than the exception.

We believe that the next significant advance of our knowledge of the impulsive phase processes will come from more observations at higher energies and with higher spatial resolutions, such as those expected from HESSI. Understanding of this new data will require a complete analysis of spatial distribution of hard X-ray emission from a flaring loop.

This paper deals with this subject in general and with the relative strength and spectral characteristics of the loop top vs. foot point emissions observed by YOHKOH in particular. The modeling of this phenomenon is discussed in §2, where we first review past relevant theoretical results and then introduce a model where plasma turbulence plays a crucial role. In §3 we describe this model and in §4 we compare results from it with the YOHKOH observations. A brief summary and discussion is given in §5.

2. Spatial Distribution of Hard X-ray Emissions

For interpretation of these observations we need the spatial distribution of hard X-ray emission during the impulsive phase by electrons as they traverse the loop from the acceleration site to the foot points. There have been several studies of this subject with some recent ones specifically designed to replicate the YOHKOH results (e.g. Masuda et al.

1994; Wheatland & Melrose 1994; Fletcher 1995; Holman 1996; and Fletcher & Martens 1998). In this section we will review these and earlier studies, most of which assume injection of some high energy electrons with an assumed energy and pitch angle distribution at the top of a symmetric closed loop.

2.1. Model Parameters

Several factors enter in the determination of the relative emissivity of the hard X-rays along the loop at different energies. The effects of almost all of these factors were first investigated in the Ph.D. thesis of J. Leach (1984) and in several related publications (Leach & Petrosian 1981 and 1983). It was assumed that the acceleration process injects electrons at the top of a loop, with the distribution $f(E, \alpha, s = 0)$, as a function of energy E (in units of the electron rest mass energy $m_e c^2$) and pitch angle α .

In this case, the most important factors are the parameters describing the distributions of the accelerated electrons (e.g. spectral index δ , the beaming direction α_b and width α_0), and the variation of plasma density $n(s)$ and magnetic field $B(s)$ along the loop. Two important parameters related to the characteristics of the plasma are $d \ln B / d \ln N$, where $N(s) = \int_0^s n(x) dx$ is the column depth measured along the loop from the injection point at $s = 0$, and N_{tr} the column depth to the transition region. One may replace the first parameter by an average convergence rate; e.g. the ratio $B(N_{tr})/B(0)$. At higher (gamma ray) energies and for microwave emission, the absolute value of the magnetic field is also important (see e.g. McTiernan & Petrosian 1990a and 1990b, and Lu & Petrosian 1989). In this section we are dealing with photon energies $k < 100$ keV where this will not be important. We now review the effects of these parameters in isolation and together.

2.2. Uniform Loops

For loops with constant field strengths, $B(s) = B_0$, the variation of the X-ray intensity along the loop becomes simple when expressed in terms of the column depth N . Figure 1, from Leach (1984), shows the variation with dimensionless column depth, $\tau = N/N_0$, of the normalized intensity of hard X-rays ($\int_0^\infty I(\tau, k) d\tau = 1$), for various photon energies k and for three models. Here $N_0 = (4\pi r_0^2 \ln \Lambda)^{-1} = 5 \times 10^{22} \text{cm}^{-2}$, where r_0 is the classical radius of the electron, $\ln \Lambda \simeq 20$ is the Coulomb logarithm. The injected electron distribution is assumed to obey $f(E, \alpha, s = 0) \propto E^{-\delta} \exp(-(\alpha - \alpha_b)^2 / \alpha_0^2)$, with $\delta = 5$. The left panel of this figure shows the effects of the degree of the beaming of the accelerated electrons for uniform magnetic field loops; $\alpha_b = 0$ and $\alpha_0^2 = 0.04, 0.4$ and ∞ (i.e. an isotropic pitch angle distribution), for curves labeled 5, 1 and 4, respectively. Leach (1984) finds that within 10 to 30%, the curves for the intermediate model ($\alpha_0^2 = 0.4$) and for $\delta = 3, 4$ and 5 can be described by

$$I(N, k) dN = \left(\frac{\delta}{2} - 1\right) \left(1 + \frac{N}{N(\alpha_0^2, k)}\right)^{-\delta/2} \frac{dN}{N(\alpha_0^2, k)}, \quad (1)$$

where $N(\alpha_0^2, k)$ is the column depth below which most of the photons with energy k originate; the intensity is constant for smaller column depths but decreases rapidly for column depths exceeding this value.

$N(\alpha_0^2, k)$ depends weakly on the pitch angle distribution of the injected electrons. For the intermediate model, Leach finds that $N(0.4, k) \simeq N_0 k^2 / (k + 1)$. For the isotropic model $N(\infty, k) \simeq 0.37 N_0 k^2 / (k + 1)$ which as expected is smaller so that the intensity begins to drop earlier. The reverse is true for the model with strong beaming along the field lines; the critical column depth is about a factor of 4 higher. Here and in what follows the photon energy k is in units of $m_e c^2$. The above expression fails at very low column depths for the last model because the Coulomb collisions gradually scatter the strongly beamed electrons into higher pitch angles, giving rise to some small, initial increases of intensity with

increasing N or τ . This dependence on both the spectral index and pitch angle distribution was further investigated by McTiernan & Petrosian (1990b) and Petrosian, McTiernan & Marschhäuser (1994) at higher photon energies, and more recently by Fletcher (1996) in an analysis involving variation of the average height of the hard X-ray emission with photon energy and model parameters.

To convert these distributions to ones in terms of distance s along the loop, we need to specify the density variation $n(s)$. For example, for a truly uniform loop $n(s) = n_0$ and $N = n_0 s$ so that the above behavior reflects the variations with s as well. In a real loop, because of the high coronal temperature, the density scale height (or more exactly $ds/d\ln n$) is expected to be much larger than the length of the loop, $L \sim 10^9$ cm, so that the constancy of the density in the coronal portion is reasonable. However, this condition fails completely below the transition region where the density first jumps abruptly and then increases exponentially with a much smaller ($\sim 10^8$ cm) scale height. For photon energies where the critical cplumn depth $N(\alpha_0^2, k) > N_{tr}$, the column depth to the transition region, we expect a nearly uniform or very slowly decreasing flux throughout the loop followed by an abrupt increase at the foot points. On the other hand for lower photon energies, or for $N(\alpha_0^2, k) < N_{tr}$ most of the emission will come from the loop rather than the foot points. Integration of equation (1) gives the ratio of emission throughout the coronal portion of the loop to that from the transition region and below it (i.e. foot points);

$$\frac{J_{Loop}}{J_{FP}} = -1 + \left(1 + \frac{N_{tr}}{N(\alpha_0^2, k)}\right)^{\delta/2-1}, \quad \delta > 2. \quad (2)$$

Since for most flares, and in particular for the YOHKOH limb flares of interest here, this ratio is less than one, the quantity N_{tr} must be less than $N(\alpha_0^2, k)$. This also means that whatever emission there is from the loop will be very nearly uniform and not concentrated towards the top of the loop.

One possible way to obtain substantial radiation from the loop top but not from the

sides of the loop, is to inject electrons with a “pancake” distribution ($\alpha_b = \pi/2$ and $\alpha_0 \ll 1$). Leach (1984) did not consider such models. The consequences of this type of distribution were considered for studies of the directivity of the high energy emissions (hard X-rays and gamma rays) by Dermer & Ramaty (1986) and McTiernam & Petrosian (1991), and in the investigation of the average height of lower energy X-ray emission by Fletcher (1996). We shall return to this possibility below.

2.3. Non-Uniform Loops

The simple spatial variation described above can be modified considerably if the plasma density and/or the magnetic field vary strongly along the loop. For example, if the density decreases from the loop top to the foot point in the coronal part of the loop, then the thin target emission from this portion being proportional to the ambient density will mimic this variation; equation (1) will still be valid, but the spatial distribution will be $I(s, k) = I(N, k)n(s)$. Such a model was proposed by Wheatland and Melrose (1995) for the YOHKOH limb flares. It is difficult to see how large density gradients can be maintained in a $T \geq 10^6 K$ plasma unless the density enhancement is a transient phenomena.

Enhancement of loop top emission can be produced more naturally in loops with converging field geometry. The field convergence increases the pitch angle of the particles as they travel down the loop, and if strong enough, can reflect them back up the loop before they reach the transition region. This increases the density of the accelerated electrons near the top of the loop giving rise to a corresponding enhancement of the bremsstrahlung emission. Such models were also investigated by Leach (1984), showing significant increases of emission from loop tops (right panel Figure 1), and by Fletcher (1996) showing increase in the average height of the X-ray emission.

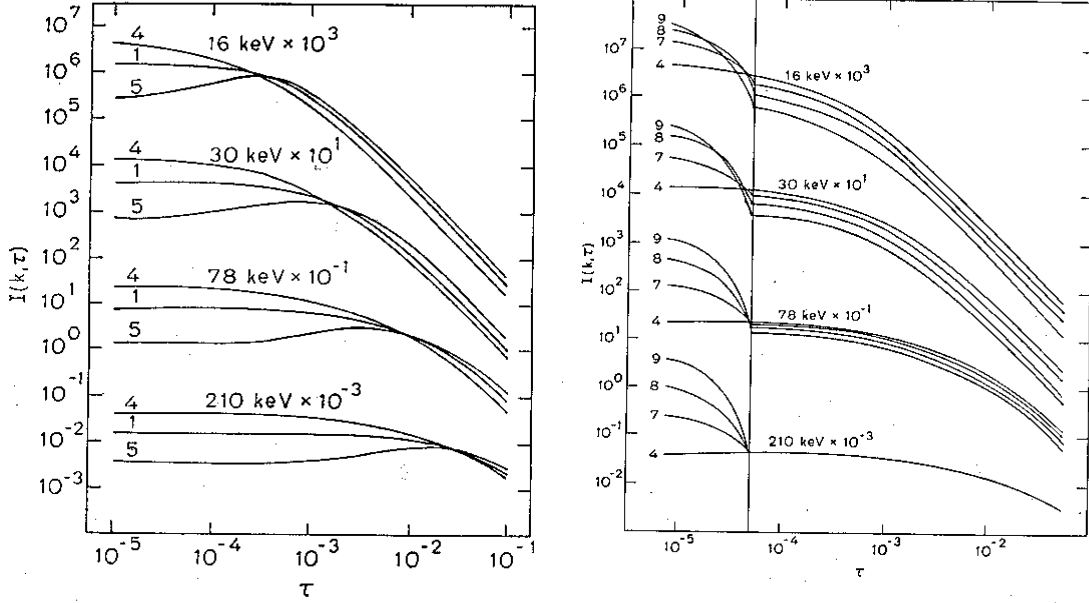


Fig. 1.— These Figures taken from the thesis of J. Leach (1984) shows the variation of normalized intensity with dimensionless column depth $\tau = N/N_0$, where $N_0 = (4\pi r_0^2 \ln \Lambda)^{-1} = 5 \times 10^{22} \text{cm}^{-2}$. The curves are labeled by the values of the photon energies and for clarity are shifted upward by the indicated amounts. *Left Panel* demonstrates the effects of the degree of beaming of the accelerated electrons; curve marked 4, 1 and 5 are for three models with values of the pitch angle distribution widths $\alpha_0^2 = \infty, 0.4$ and 0.04 , respectively. The magnetic field is uniform and the spectral index $\delta = 5$. *right Panel* shows the effects of magnetic field convergence for models with $\delta = 5$ and isotropic pitch angle distribution; the field convergence rate is chosen to give ratios of magnetic field strength at the transition region to that at the top of the loop $B(N_{tr})/B(0) = 1, 2, 5$ and 25 for curves with labels 4, 7, 8 and 9, respectively.

Finally, trapping of electrons near the loop top can also come about by an enhanced pitch angle scattering. The primary reason that the hard X-ray bremsstrahlung emission is described by the smooth and monotonic expression of equation (1) is due to the fact that for Coulomb collisions (the dominant interaction process for nonrelativistic energies) the mean free paths for the pitch angle scattering and energy loss are comparable and approximately equal to $\lambda_{\text{Coul}} = -vE/\dot{E}_{\text{Coul}}$ where $v = \beta c$ is the electron velocity and $\dot{E}_{\text{Coul}} = -4\pi r_0^2 n \ln \Lambda / \beta$ is the energy loss rate (in units of $m_e c^2$). However, if there exists another scattering agent with $\lambda_{\text{scat}} \ll \lambda_{\text{Coul}}$ then electrons undergo many pitch angle scatterings before they lose a substantial amount of their energy. Furthermore, if $\lambda_{\text{scat}} \ll L$, the size of the region near the top of the loop, the electrons will be trapped for a time $T_{\text{esc}} \simeq \frac{L}{v} \times \frac{L}{\lambda_{\text{scat}}} \gg \frac{L}{v}$, achieve an isotropic pitch angle distribution ($\alpha_0 \rightarrow \infty$), and give rise to enhanced emission from the loop top. The ratio of the loop top emission compared to emission from other parts of the coronal portion of the loop (which do not contain such a scattering agent but are of comparable length) will be approximately $J_{LT}/J_{Loop} \simeq L/\lambda_{\text{scat}}$, in which case we may detect emission only from the top of the loop and the high density foot points, but not from the legs of the loop.

In summary, in order to have the bulk of the emission to come from the foot points we need $N_{tr} \ll N(\alpha_0^2, k) \simeq N_0 k^2 / (k + 1)$, which is equivalent to having $\lambda_{\text{Coul}} \gg L$ in the coronal parts of the loop. And in order to enhance the emission near the loop top without doing the same from the rest of the loop we require $\lambda_{\text{scat}} \ll L$. A possible scattering agent which could satisfy this condition is plasma turbulence. If this is the case, however, one must also include the possibility of acceleration of the particles by the same plasma turbulence.

3. Stochastic Acceleration

Stochastic acceleration of particles by plasma waves or turbulence, a second order Fermi acceleration processes, is one of the leading candidates for production of nonthermal particles in solar flares. Their role in accelerating protons and ions have been investigated in some simplified models by Ramaty and collaborators (see e.g. Ramaty 1979 and Ramaty & Murphy 1987). Based on some theoretical arguments and on new higher spectral and spatial resolution data (such as that from the events under consideration here) we have argued that stochastic acceleration by plasma turbulence is the most promising process for acceleration of flare electrons (Petrosian 1994 and 1996). Similar arguments have been put forth by Schlickeiser and collaborators (Schlickeiser 1989; Bech et al. 1990), and Miller and collaborators (Miller 1991; Miller, LaRosa & Moore 1996; Miller & Reames 1996). In a combined acceleration, transport and radiation model we have compared theoretical spectra with observations (Petrosian et al. 1994; Park, Petrosian & Schwartz 1997, hereafter **PPS**) and have shown that some of the observed X-ray and gamma ray spectral features, in particular the deviations from a simple power law, can be most naturally explained with such models. PPS explore various acceleration models and include the effects due to Coulomb collisions and synchrotron losses and determine model parameters for several flares observed by GRS on SMM, and BATSE and EGRET on C-GRO. Here we use the same formalism to determine the spatial distribution of hard X-rays. We first review the relevant aspects of this model and then compare its predictions with the YOHKOH observations.

3.1. Model Description

The exact solution of the combined acceleration, transport and radiation processes requires solution of the time dependent coupled kinetic equations for waves and particles. This is beyond the scope of this work and is not warranted for comparison with the existing

data. We therefore make the following simplifying and somewhat justifiable assumptions. We shall return to the possible breakdown of these assumptions in the summary section.

a) We assume that the flare energizing process, presumably magnetic reconnection, produces plasma turbulence throughout the impulsive phase at a rate faster than the damping time of the turbulence, so that the observed variation of the impulsive phase emissions is due to modulation of the energizing process. This assumption decouples the kinetic equation of waves from that of the electrons. We assume that the turbulence is confined to a region of size L near the top of the flaring loop.

b) The requirement $\lambda_{\text{scat}} \ll L$ indicates that the plasma electrons will undergo repeated pitch angle scattering in the acceleration region so that a nearly isotropic pitch angle distribution is established. Therefore we need to contend only with diffusion in momentum (or energy) due to the turbulence and energy losses by other processes. The kinetic equation for diffusion in the acceleration region is (for further details see Park & Petrosian 1995 and 1996, and PPS)

$$\frac{\partial f}{\partial t} = \frac{\partial^2}{\partial E^2} [D(E)f] - \frac{\partial}{\partial E} [(A(E) - |\dot{E}_L|)f] - \frac{f}{T_{\text{esc}}(E)} + Q(E). \quad (3)$$

Here D and A are the diffusion and systematic acceleration coefficients due to the stochastic process which are obtained from the standard Fokker-Planck equation (Chandrasekhar 1943), and

$$\dot{E}_L = \dot{E}_{\text{Coul}} + \dot{E}_{\text{synch}} = -4\pi r_0^2 c n \ln \Lambda / \beta - 4r_0^2 B^2 \beta^2 \gamma^2 / 9m_e c^2 \quad (4)$$

describes the Coulomb and synchrotron energy loss rates (in units of $m_e c^2$). For the source function, $Q(E)$, we use a Maxwellian distribution with temperature, $kT = 1.5$ keV.

c) We will be comparing model results with “maps” integrated over a time which is much longer than all other time scales such as the traversal time $\tau_{tr} = \frac{L}{c\beta} = 0.03\text{s}(\frac{L}{10^9\text{cm}})\frac{1}{\beta}$, the escape time $T_{\text{esc}} \simeq (\frac{L}{\lambda_{\text{scat}}})\tau_{tr}$, or the acceleration time $\tau_{ac} \simeq \frac{D(E)}{E^2} \simeq \frac{A(E)}{E}$. Therefore, we can ignore the time dependence and use the steady state solution ($\frac{\partial f}{\partial t} = 0$).

d) Following PPS we use the whistler model but mostly a more general model with

$$D(E) = \mathcal{D}\beta(\gamma\beta)^{q'}, \quad A(E) = \mathcal{D}(q' + 2)(\gamma\beta)^{q'-1}, \quad T_{\text{esc}}(E) = \mathcal{T}_{\text{esc}}(\gamma\beta)^s / \beta + L/(\beta c\sqrt{2}). \quad (5)$$

Here we have added some average traverse time as a minimum escape time and have used a different notation than PPS; our q' plays the role of the parameter q in PPS, while we reserve q for the spectral index of the (assumed) power law distribution for the plasma wave vectors (PPS use the symbol \tilde{q} for this latter index). Our notation here agrees with that in Dung & Petrosian (1994) and Pryadko & Petrosian (1997, 1998 and 1999). As shown in these papers, the rate of acceleration is proportional to \mathcal{D} which in turn is proportional to the electron gyrofrequency, Ω_e , and the level of turbulence $f_{\text{turb}} = 8\pi\mathcal{E}_{\text{tot}}/B^2$, where \mathcal{E}_{tot} is the total energy density of turbulence. In the Whistler model \mathcal{D} and \mathcal{T}_{esc} are related and $s = q' = q - 2$. For a more complete analysis one should use the numerical results given in the last four references which evaluate the total contributions from all plasma modes. The existing data do not warrant considerations of such details. Consequently, we shall leave such details for the interpretation of better data to be obtained by HESSI. However, we shall choose the parameters in the above expressions so that the relevant parameters qualitatively behave like the ones from these numerical results.

The spectrum of the accelerated particles depends primarily on the three dimensionless parameters

$$\zeta_{\text{esc}} = \mathcal{D}\mathcal{T}_{\text{esc}}, \quad \zeta_{\text{Coul}} = \mathcal{D}/(4\pi r_0^2 cn \ln\Lambda), \quad \zeta_{\text{synch}} = 9\mathcal{D}m_e c^2 / (4r_0^2 c B^2), \quad (6)$$

on the exponents s and q' , and weakly on the size L (only at very low energies). Figure 2 shows some representative spectra of the electrons in the acceleration site, $f_{AS}(E)$, obtained from solving equation (3). If we ignore the losses (i.e. for ζ_{Coul} and $\zeta_{\text{synch}} \gg 1$) the only parameters affecting the spectrum are ζ_{esc} and $s + q'$ which determine the amplitude and the energy dependence of the ratio of the escape time to the acceleration time; $R_{\text{esc}} \equiv \mathcal{D}\mathcal{T}_{\text{esc}}/E^2$.

In the left panel of Figure 2 we use $q' = 1.7$, $s = 1.5$ so that this ratio decreases with E at nonrelativistic energies but increases at extreme relativistic values mimicking the steep turbulence spectrum ($q = 3$) results of Pryadko & Petrosian (1997). The solid curves (labeled A to E) show the spectra for five values of $\zeta_{\text{esc}} = 0.0025, 0.05, 0.1, 0.2$ and 0.4 , respectively. Other parameters are kept constant, except we vary the density so that $n\mathcal{T}_{\text{esc}} \propto \zeta_{\text{esc}}/\zeta_{\text{Coul}}$ remains constant. These spectra are steep throughout for small values of ζ_{esc} , but they flatten with increasing ζ_{esc} and may acquire a positive power law index at relativistic energies. All spectra eventually fall off exponentially when the synchrotron loss rate becomes comparable to the acceleration rate; i.e. $R_{\text{synch}} \equiv -D(E)/(E\dot{E}_{\text{synch}}) \rightarrow 1$. Using relativistic approximation it can be shown that this happens for energies beyond the critical energy $E_{\text{synch}} = \zeta_{\text{synch}}^{1/(3-q')}$. This effect is evident more dramatically from comparison of the two dotted curves labeled C_{B1} and C_{B2} with the heavy solid line C which have same parameters except the magnetic field is set to 100, 1000 and 300, respectively. In a similar manner, the Coulomb losses steepen the spectrum below the critical energy E_{Coul} obtained from the equality $R_{\text{Coul}} \equiv -D(E)/(E\dot{E}_{\text{Coul}}) = 1$. For nonrelativistic energies $E_{\text{Coul}} = 2^{-(2+q')/q'} \zeta_{\text{Coul}}^{-2/q'}$. This effect can be seen by comparing the solid curve C with the dashed lines labeled C_{n1} and C_{n2} which are for three different values of density. For a complete listing of the parameters used in this and subsequent related figures see Table 1. (For further discussion of these effects see Hamilton & Petrosian 1992 and Bech et al. 1990).

In the right panel of Figure 2 we show the effect of the variation of the energy dependence of the ratio R_{esc} . Here we vary the exponent s and keep all other parameters constant and equal to their values used for the model represented by the heavy solid line labeled C in both panels of Figure 2. For larger exponent the acceleration time becomes shorter than the escape time at high energies and gives rise to a larger number of high energy electrons. For lower values of this exponent the ratio R_{esc} decreases monotonically with energy both at nonrelativistic and extreme relativistic cases. This behavior is qualitatively

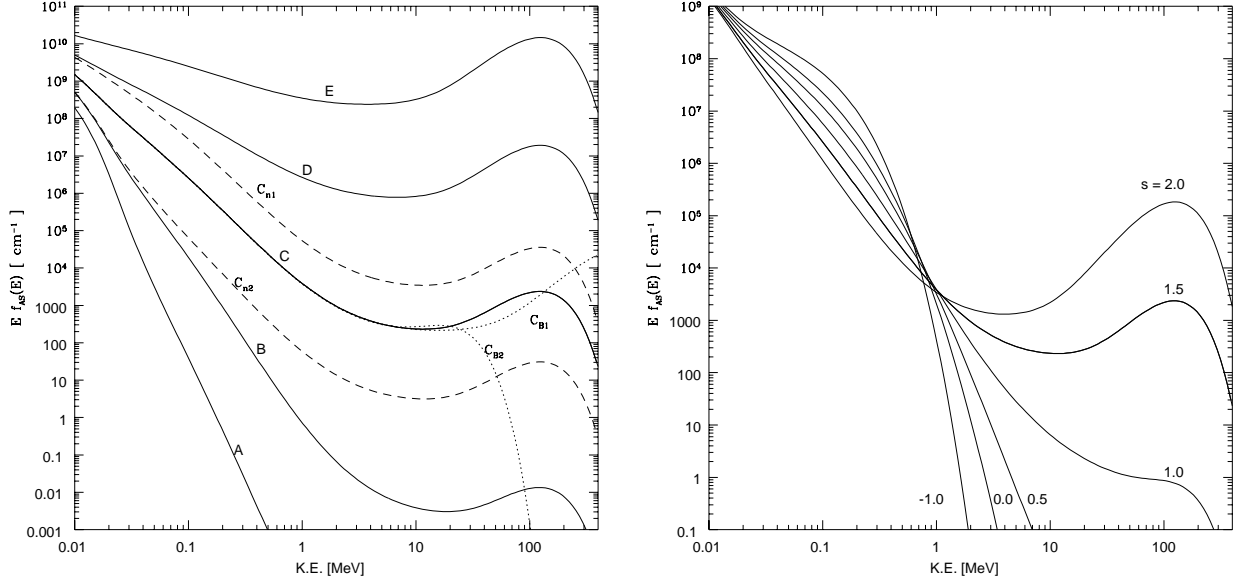


Fig. 2.— Representative spectra of the accelerated electrons for two different kinds of models. For convenience we plot product of energy times spectral density. *Left Panel:* The solid lines (A to E) are for models with $\zeta_{\text{esc}} = 0.0025, 0.005, 0.01, 0.02$ and 0.04 , respectively. We use a constant ratio of $\zeta_{\text{Coul}}/\zeta_{\text{esc}} = 167$ or $n\mathcal{T}_{\text{esc}} = 10^{10} \text{ cm}^{-3} \text{ s}$, so that the proportionality factor in equations (15) and (17) is constant. We use $B = 300\text{G}$ or $\zeta_{\text{synch}} = 420$, $q' = 1.7$ and $s = 1.5$; these exponent are chosen to qualitatively mimic the behavior of the Fokker-Planck coefficients for a steep spectrum of turbulence ($q = 3$) calculated by Pryadko & Petrosian (1997). The two dashed lines C_{n1} and C_{n2} are same as model C except the density is lower and higher by factor of 2, respectively. The dotted lines labeled C_{B1} and C_{B2} are for magnetic fields of 100 and 1000 G, respectively. The parameters for the various curves can also be found in Table 1. *Right Panel:* Curves are labeled by the value of the exponent s showing the effects of the energy dependence of the ratio of the acceleration to escape times; i.e. the exponent $s + q'$. All other parameters same as model C (heavy solid lines) in both panels.

similar to what one may obtain for a flat spectrum of turbulence such as the case $q = 5/3$ in Pryadko & Petrosian (1997). In this case the electrons escape too quickly for a substantial acceleration to high energies. Consequently, the spectra fall off steeply at high energies. This will be true for all values of ζ_{esc} used in Figure 2. However, as expected the spectra flatten at low energies. The extremely efficient acceleration of low energy particles is responsible for this behavior in these models. These two figures demonstrate that a rich variety of accelerated electron spectra are possible by this mechanism.

Table 1
Model Parameters for left panels of Figures 2, 3, 5 and 6

Label	$\mathcal{T}_{esc}[s]$	$n[cm^{-3}]$	$B[gauss]$	ζ_{esc}	ζ_{Coul}	ζ_{synch}	$E_{Coul}[m_e c^2]$	$E_{synch}[m_e c^2]$
A	0.05	2×10^{11}	300	0.0025	0.417	421	1.68	104
B	0.10	1×10^{11}	300	0.005	0.833	421	0.88	104
C	0.20	5×10^{10}	300	0.01	1.667	421	0.26	104
D	0.40	2.5×10^{10}	300	0.02	3.333	421	0.058	104
E	0.80	1.25×10^{10}	300	0.04	6.667	421	0.025	104
C_{B1}	0.20	5×10^{10}	100	0.01	1.667	3788	0.26	565
C_{B2}	0.20	5×10^{10}	1000	0.01	1.667	37.9	0.26	16.4
C_{n1}	0.20	2.5×10^{10}	300	0.01	3.333	421	0.058	104
C_{n2}	0.20	1×10^{11}	300	0.01	0.833	421	0.88	104

$$\mathcal{D} = 0.05[s^{-1}], L = 1 \times 10^9 [cm], q' = 1.7, s = 1.5, Q_0 = 1 \times 10^{12} [\text{particles/sec}]$$

In what follows we will explore the model parameters represented in the left panel of Figure 2 because of its diversity and because the spectral fittings by PPS obtained a range of values closer to this region of the parameter space.

The escaping electrons will have a nearly isotropic pitch angle distribution in the

downward direction and a spectral flux equal to $F_{\text{esc}} = Lf_{AS}/T_{\text{esc}}$. As we shall see below for the calculation of the thick target bremsstrahlung emission by these electrons at the foot points we shall need the integral of this flux divided by the loss term. We call this f_{thick} :

$$f_{\text{thick}} = -\frac{1}{\dot{E}_L} \int_E^\infty \frac{f_{AS}}{T_{\text{esc}}} dE \quad (7)$$

This spectrum is shown in Figure 3 for the same parameters used in Figure 2. As evident there is considerable differences between f_{AS} and f_{thick} . For simple power laws, i.e. for low values of ζ_{esc} , the power law index of spectrum relevant for the foot points is expected to be smaller (in absolute value, i.e. flatter) than that of the spectrum at the acceleration site by $2 - s/2$ and $1 - s$ for nonrelativistic and extreme relativistic limits, respectively. Thus, in general, unless the exponent s for the escape term is greater than 4, we expect the foot point spectrum to be flatter than that at the acceleration site. For intermediate values of ζ_{esc} both f_{AS} and f_{thick} undergo several changes in their spectral indices. Both spectra undergo further variations at low and high energies where the effects of the Coulomb and synchrotron losses come in. These differences between the two spectra will produce similar differences between the emissions from the acceleration site and the foot points.

3.2. Bremsstrahlung Emission

We now evaluate the emission from the acceleration site in addition to that from the coronal portion of the loop and the foot points discussed earlier.

The Thin Target bremsstrahlung photon number spectrum from the acceleration site can be found from

$$J_{AS}(k) = L \int_k^\infty dE f_{AS}(E) \beta c n_{AS} \frac{d\sigma}{dk}(E, k), \quad (8)$$

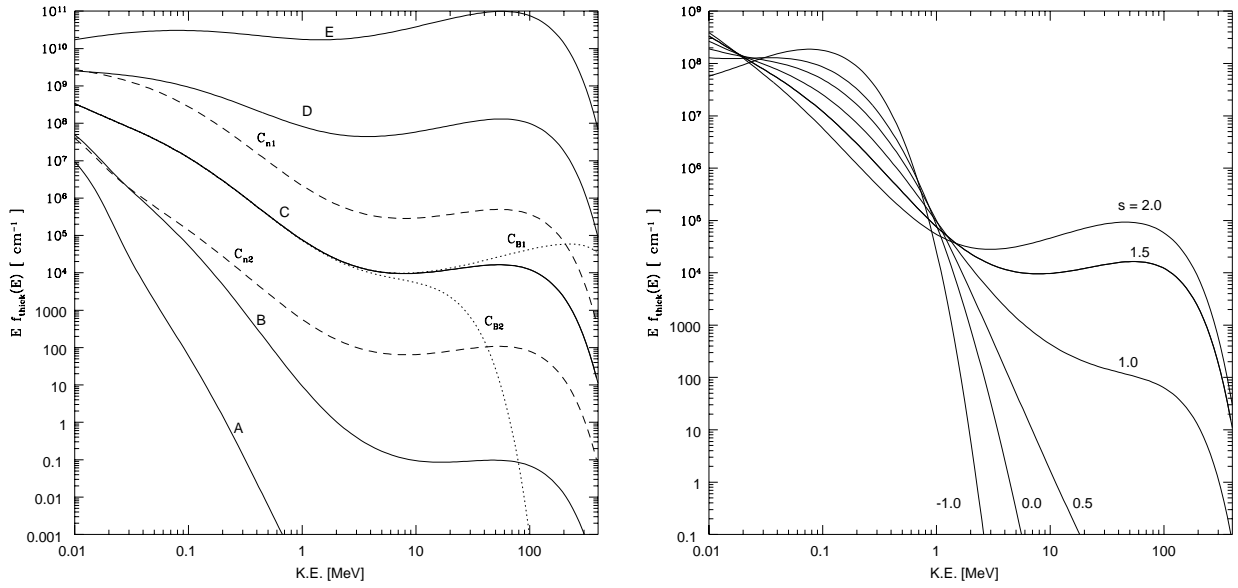


Fig. 3.— The effective electron spectra at the thick target (foot points) as defined by equation (7) for the models of Figure 2 or the parameters given in Table 1. In general these spectra are flatter than those in Figure 2.

where n_{AS} is the background density in the acceleration site, $d\sigma/dk$, given by Koch & Motz (1959, eq. [3BN]), is the relativistically correct, angle integrated, bremsstrahlung cross section, L is the length of the acceleration region at the top of the loop so that $V = A \times L$ is the volume of the acceleration region. The spectrum f_{AS} is integrated over the cross-sectional area of the loop so that the area A only affects the overall normalization of the photon spectrum and can be absorbed into the source function Q in equation (3).

In the nonrelativistic and extreme relativistic limits the bremsstrahlung cross section can be approximated as

$$\frac{3\beta^2 k}{16\alpha r_0^2} \frac{d\sigma}{dk} = \begin{cases} \ln \frac{1+\sqrt{1-x}}{1-\sqrt{1-x}} & \text{for } k, E \ll 1, \\ \left(\ln \frac{2k}{\sqrt{e}} + \ln \frac{1-x}{x^2} \right) (1-x + \frac{3}{4}x^2) & \text{for } E \gg 1. \end{cases} \quad (9)$$

where α is the fine structure constant and $x = k/E \leq 1$ is the ratio of photon to electron energies. Figure 4 compares these expressions with the more accurate 3BN formula of Koch and Motz (1959). The nonrelativistic approximation is valid only for very low values of both k and E . Its range of validity decreases rapidly with increasing k . For $\ln k = -3$, (photon energy of ~ 188 keV) it is within $\leq 10\%$ of the exact value for electron energies $E < 1$. Therefore, some caution is required in using this approximation for photon energies ≥ 100 keV. On the other hand, the extreme relativistic approximation is not only valid for k and $E \gg 1$ but also at nonrelativistic photon energies as long as $E \gg 1$. For $k \sim 1$ it requires $E > 3$ for a 10% or better accuracy.

As mentioned above a nearly isotropic (in the downward direction) flux of electrons, $F_{esc}(E) = Lf_{AS}/T_{esc}$, will escape the acceleration site and will be transported along the loop to the foot points, emitting bremsstrahlung radiation with the spatial distribution described in the previous section (e.g. eq.[1]). As long as N_{tr} , the column depth from the edge of the acceleration site to the transition region, is significantly less than $N(\alpha_0^2, k) \simeq N_0 k^2 / (k + 1)$, most of this radiation will come from the foot points. As stated previously, this condition

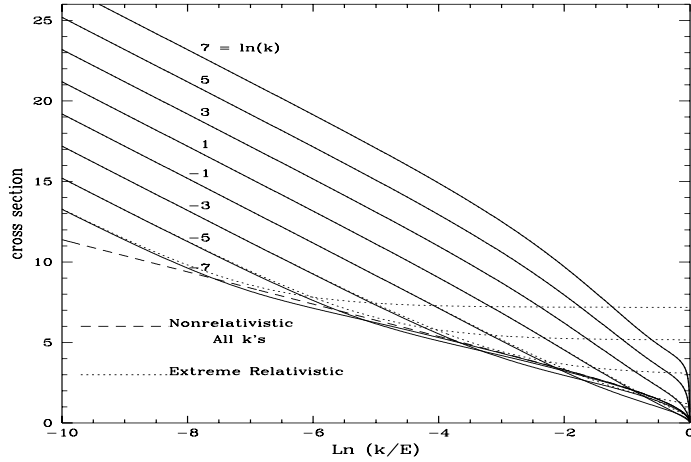


Fig. 4.— Comparison of the extreme relativistic (dotted lines) and the nonrelativistic (dashed lines) approximations for the bremsstrahlung cross section given by the right hand side of equation (9) with the more accurate formula given in Koch & Motz (1959, eq. [3BN]) (solid lines).

requires that λ_{loss} ($= \lambda_{\text{Coul}}$ for nonrelativistic electrons) to be much larger than the length of the leg of the loop (which is of the order of L). This means that the electrons are moving essentially freely downward and their isotropic distribution is preserved even if the field converges: The field convergence has no significant effect because the flux integrated over the tube cross-section is conserved (see e.g. Leach & Petrosian 1983). Thus, most of the radiation will come from the foot points in a thick target source.

The Thick Target bremsstrahlung spectrum of this source is obtained from the following well known expression (see e.g. Petrosian 1973)

$$J_{FP}(k) = L \int_k^\infty dE f_{\text{thick}} \beta c n \frac{d\sigma}{dk}(E, k). \quad (10)$$

The density n here and in \dot{E}_L used in equation (7) refer to the background density at the foot points. Here the density may exceed 10^{12} cm^{-3} so that for field strengths of $B \simeq 300\text{G}$ the synchrotron losses become important only for Lorentz factors $\gamma \geq 10^2$, which

is beyond even the EGRET observations considered in PPS. Consequently, for all relevant energies, in particular for nonrelativistic electrons under consideration here, we have

$\frac{\dot{E}_L}{n} \simeq \frac{\dot{E}_{cool}}{n} = -4\pi r_0^2 \ln \Lambda c/\beta$ which means that the foot point emission will be independent of the plasma parameters n and B (except, of course, for the dependence of f_{thick} on these quantities).

3.3. Loop Top vs. Foot point Emission

We now determine the intensity and spectral differences between the acceleration site and foot point emissions. In what follows we first derive some analytic expressions using power law approximations for the electron spectra and ignoring the slowly (logarithmic) varying part of the cross-section (right hand side of equation [9]). We then present some numerically calculated spectra using the exact expressions for the electron spectra and the cross section. If the spectrum of the accelerated electrons is a relatively steep power law ($f(E) = \kappa E^{-\delta}, \delta \gg 1$), then most of the emission at photon energy k will come from electrons with energies E just slightly above k . The bremsstrahlung emission can be then approximated as

$$J(k) \simeq \kappa L \frac{16}{3} \alpha r_0^2 n c \begin{cases} k^{-\delta-\frac{1}{2}}/(\sqrt{2}(\delta-\frac{1}{2})) & k \ll 1, \\ k^{-\delta}/(\delta-1) & k \gg 1. \end{cases} \quad (11)$$

However, for $\delta < 1$ most of the contribution at photon energy k will come from the highest energy electrons that this spectrum extends to. In our case this will be roughly the energy E_{synch} defined in previous section above which the electron spectra decrease rapidly. The photon spectrum in this case can be approximated as

$$J(k) \simeq \kappa L \frac{16}{3} \alpha r_0^2 n c \frac{E_{\text{synch}}^{1-\delta}}{1-\delta} k^{-1} \begin{cases} 1 + \frac{(\delta-1)k^{-\delta+\frac{1}{2}}}{\sqrt{2}(\delta-\frac{1}{2})E_{\text{synch}}^{1-\delta}} & k \ll 1, \\ 1 - (k/E_{\text{synch}})^{1-\delta} & E_{\text{synch}} \gg k \gg 1. \end{cases} \quad (12)$$

which for most practical purposes (for $k > 0.03$ and $E_{\text{synch}} > 10^3$) gives $J(k) \propto k^{-1}$.

Application of these equations to the emission from the acceleration site is straight forward because the spectrum of the accelerated electrons for most of the relevant energy range (specially those of interest here) can be approximated with simple broken power laws. Therefore, the emission J_{AS} is obtained from the above expressions with the replacing of n by n_{AS} , the density at the acceleration site. For low values of ζ_{esc} we have steep electron spectra and a photon spectrum given by equation (11). For high values the photon spectra are expected to obey equation (12). The dashed line in Figure 6 shows the photon spectra of the acceleration site for the same model parameters as Figures 3 and 4 and demonstrate both of the above behaviors.

The emission from the foot points is more complicated involving both T_{esc} and \dot{E}_L . If the spectrum at the acceleration site, $f_{AS}(E)$, is relatively steep, which would be the case for $\zeta_{\text{esc}} \ll 1$, and/or if $s + q'$ is small, then the effective electron spectrum for **the thick target** emission, equation (7), can be approximated roughly as

$$f_{\text{thick}} \simeq 1/(-\dot{E}_L T_{\text{esc}}) \int_E^\infty f_{AS}(E') dE' = -\kappa E^{-\delta+1}/((\delta-1)\dot{E}_L T_{\text{esc}}(E)). \quad (13)$$

Substitution of this in equation (10), and again ignoring the variation of T_{esc} and the cross section, we find the following rough approximation for the foot point emission at all k and for $\delta > (5-s)/2$.

$$J_{FP} \simeq \kappa L \frac{16}{3} \frac{\alpha}{4\pi \ln \Lambda} \frac{k^{-\delta+1}}{T_{\text{esc}}(k)} \frac{1}{(\delta-1)(\delta-2)}. \quad (14)$$

However, as evident from Figures 2 and 3 for high acceleration rates and/or slow

escape ($R_{\text{esc}} \gg 1$) the accelerated electron spectrum flattens. In this case most of the contribution to the integrals for f_{thick} and for J_{FP} (eqs. [7] and [10], respectively) will come from the highest energy electrons and the photon spectrum, aside from the logarithmic and other slowly varying terms, will again be proportional to k^{-1} . These behaviors are seen in Figure 5 where we plot the spectra of the foot point source (the solid lines) for the same parameters as the previous figures.

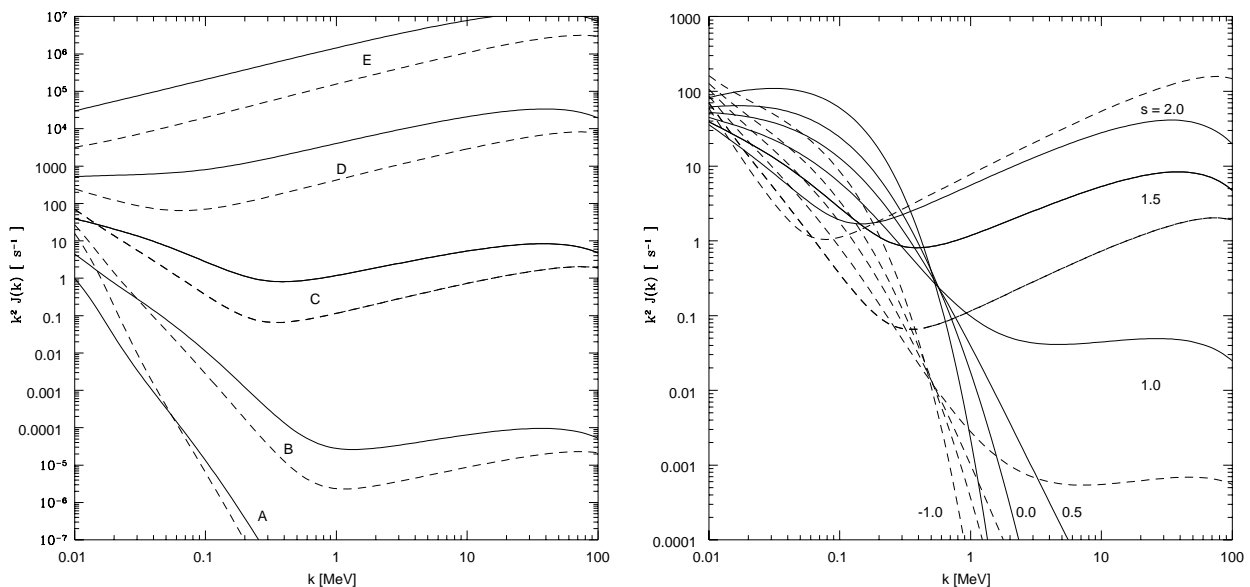


Fig. 5.— Thick target or foot point (solid lines) and thin target or acceleration site (dashed lines) photon spectra (multiplied by k^2 , for convenience) for the models of Figure 2 or the parameters given in Table 1. Note that for high values of s and/or ζ_{esc} both spectra vary as $J(k) \propto k^{-1}$ shown in equation (12).

Using these simple approximations we can calculate the ratio of the foot point to loop top emissions. It is easy to show that in both nonrelativistic and extreme relativistic regions, and for steep spectra (small ζ_{esc}) this ratio (obtained from eqs. [14] and [11]) can

be given by the simple expression

$$\frac{J_{FP}}{J_{AS}} \simeq \frac{\tau_{\text{Coul}}(k)}{T_{\text{esc}}(k)} = \frac{\zeta_{\text{Coul}}}{\zeta_{\text{esc}}} \begin{cases} 2^{(2-s)/4} k^{2-s/2} & k \ll 1, \\ k^{1-s} & k \gg 1, \end{cases} \quad (15)$$

where we have neglected terms like $\delta - 1$, $\delta - 2$, etc. and have defined the Coulomb collision time scale

$$\tau_{\text{Coul}}(k) \equiv - \left(\frac{E}{\dot{E}_{\text{Coul}}} \right)_{E=k} = (4\pi r_0^2 \ln \Lambda n_{AS} c)^{-1} \begin{cases} \sqrt{2} k^{3/2} & k \ll 1, \\ k & k \gg 1. \end{cases} \quad (16)$$

In addition to their simplicity, these expressions show that in case of relatively slow acceleration or rapid escape the ratio of the emission from the acceleration site to that of the foot points depends only on the product of the density and the escape rate ($n\mathcal{T}_{\text{esc}} \propto \zeta_{\text{Coul}}/\zeta_{\text{esc}}$) in the acceleration site and is independent of the rest of the parameters of the loop or flare plasma. This ratio is also independent of the acceleration rate $D(E)$ or the acceleration process as a whole. It is applicable to any acceleration model which produces a nearly isotropic distribution of electrons with a relatively steep spectrum.

For larger values of ζ_{esc} and flatter electron spectra both the acceleration site and foot point spectra become proportional to k^{-1} so that the ratio becomes independent of the photon energy (except at high energies where synchrotron losses dominate).

$$\frac{J_{FP}}{J_{AS}} \propto \frac{\tau_{\text{Coul}}(E_{\text{synch}})}{T_{\text{esc}}(E_{\text{synch}})} \propto \frac{\zeta_{\text{Coul}}}{\zeta_{\text{esc}}} \quad (17)$$

Figure 6 shows the variation of this ratio with the photon energy and other model parameters. Both a relatively constant ratio (expected for high ζ_{esc} , e.g. curve *E*), and rising-and-falling ratios similar to that expected from equation (15) (curves *A* to *C*) are present in this figure. However, because in most cases the electron spectra (f_{AS}, f_{thick}) suffer many deviations from pure steep power laws, the numerical results deviate significantly from the simple analytic expressions (except, perhaps at extreme high and low values of

ζ_{esc}) and show sensitivity to other parameters. This fact and the diversity of the shapes shows that, in general, the relative strengths and spectral shapes of the foot point and loop top emissions can be good diagnostic tools for the investigation of the acceleration, escape and energy loss processes.

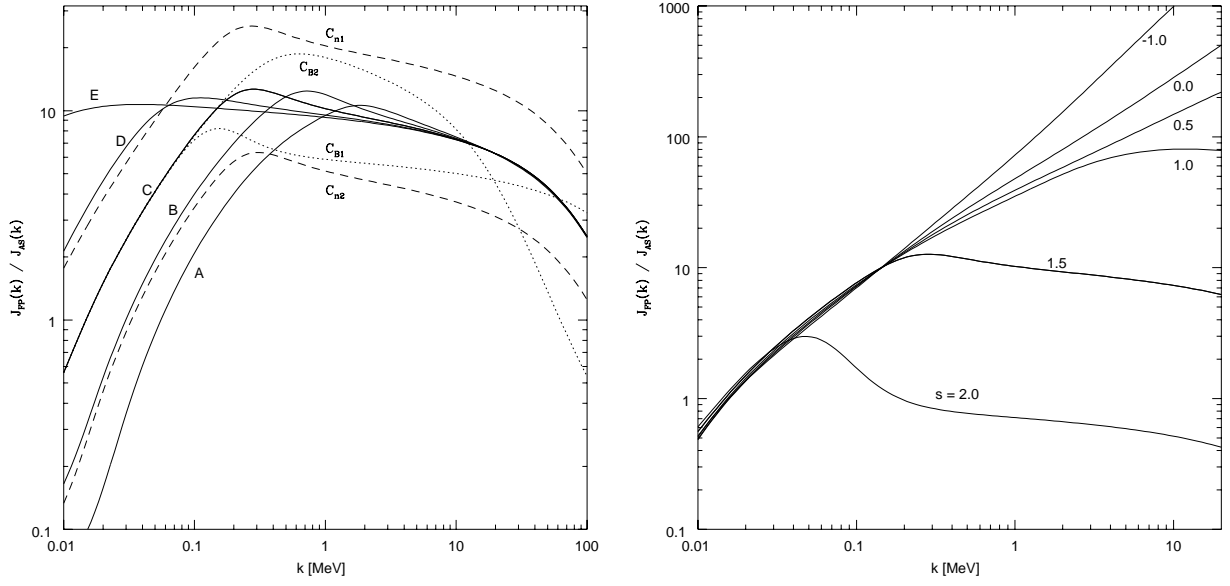


Fig. 6.— The ratio of emission from the foot points to the loop top as a function of photon energy for the models of Figure 2 or the parameters given in Table 1. Note the presence of both rise-and-fall and nearly constant behaviors in the *left panel* as expected from equations (15) and (17). Also note near independence from s of the ratio at low energies in the *right panel* except for high values of s .

4. Comparison With YOHKOH Data

In this section we compare some of the model results with the characteristics of the limb flares observed by Masuda (1994). As mentioned in §1, six out of ten flares studied

showed detectable emission from top of the loop as well as the usual foot point emission. We use the ratio of foot point to loop top emission in the the energy bands of YOHKOH and the spectral indices whenever these are available.

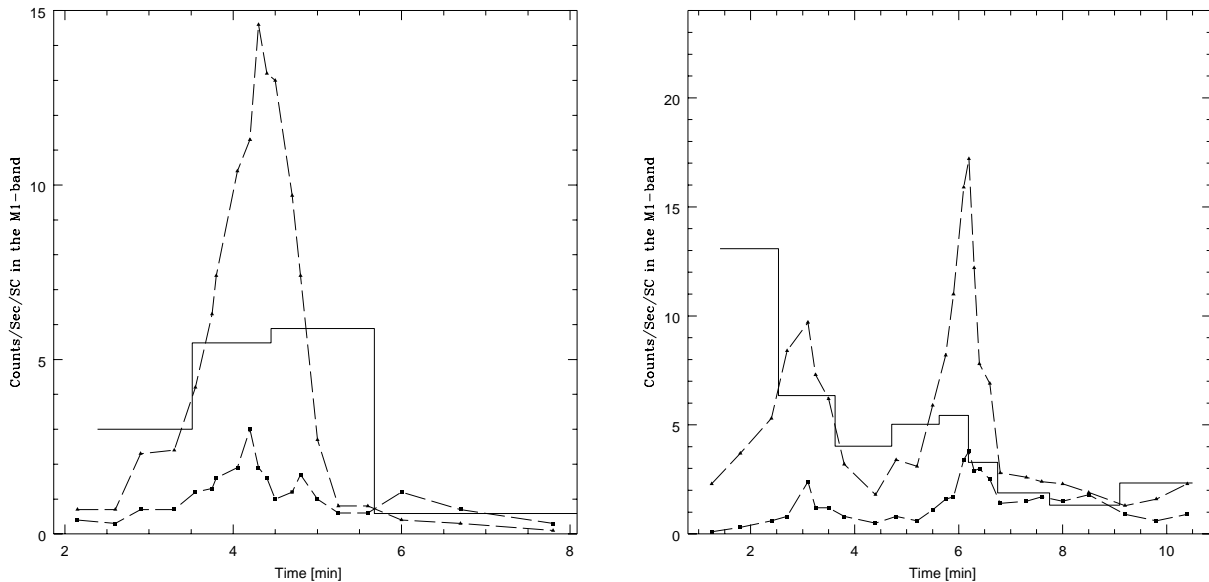


Fig. 7.— The time profiles of two flares as seen by YOHKOH in the M1 band (23-33 keV). The triangles represent the foot point flux and the squares represent the loop top flux. The solid histogram gives the ratio of the foot point to the loop top fluxes: *Left Panel*: January 13, 1992; *Right Panel*: October 4, 1922. From Masuda (1994).

Figures 7 show the observed variation with time of the above mentioned ratio for channel M1 (23-33 keV) in two flares taken from Masuda (1994). As evident when there is sufficient signal from both sources the ratio is always greater than one and averages around 5. Alexander & Metcalf (1997) have reanalyzed the January 13, 1992 flare using a different image reconstruction technique. They obtain slightly different light curves and a variable ratio in the range 3 to 4. Of course there is a strong observational selection bias here; the ratio is much larger than this for flares with undetectable emission from the loop top. There

should, however, be no strong bias against flares with values of this ratio less than one. In general, as the flare progresses the ratio tends to decrease (and becomes equal or less than one specially in the L channel; 14-23 keV). Most of this trend is probably due to increasing thermal emission from the loop tops by the evaporated plasma. But some of it could be due to changes in the acceleration or other flare parameters.

Masuda also calculates average photon spectral indices by fitting a power law to the photon number fluxes in two adjacent channels. In Table 2 we present some of these values for channels M1 and M2 from the foot point and loop top sources. In general the spectra appear to be steep. Some of this could be due to contamination by thermal plasma especially for flares where the impulsive phase is not well isolated from the thermal phase. We will ignore values greater than 6. Furthermore, because of the low counts the error bars on these values (not given in Masuda 1994) must be considerable. Alexander & Metcalf (1997) carry out a more detail analysis of the spectra of January 13, 1992 flare. They give directly the values of the power law index of the injected electrons in generic thin and thick target models. Using equation (8) and ignoring the logarithmic dependence in equation (9) it is easy to show that for electron spectrum $f \propto E^{-\delta}$, the thin target photon spectrum will be $J \propto k^{-\delta-1/2}$. For the peak of the emission in channel M1 Alexander & Metcalf give $2.5 < \delta_{LT} < 3.7$ and $3.2 < \delta_{FP} < 4.4$, which translate to average photon indices of 3.6 and 4.3 for loop top and foot point sources, respectively. Considering the error bars, this is in good agreement with the Masuda results.

TABLE 2

Photon spectral indices for selected flares from Masuda (1994)

Date	FootPoint	LoopTop
91/12/02	6.3	5.5
91/12/15	3.9	-
92/01/13	4.0	4.1
92/04/01	3.7	-
92/10/04	3.4	5.2
92/11/23	4.6	6.3

In what follows we try to get a rough measure of model parameters using the overall ranges of the intensity ratios and spectral indices. Figure 8 shows the intensity ratio, J_{FP}/J_{LT} , in the M1 band as a function of acceleration rate parameter \mathcal{D} for three different values of the escape time parameter \mathcal{T}_{esc} and density. For small values of \mathcal{D} or ζ_{esc} , i.e. for slow acceleration rates, this ratio varies rapidly and is sensitive to density and not the escape time \mathcal{T}_{esc} . For $\mathcal{D} > 0.1$ (i.e. larger ζ_{esc}) this ratio approaches an asymptote whose value depends linearly on the ratio $\zeta_{Coul}/\zeta_{esc} \propto (n\mathcal{T}_{esc})^{-1}$, in agreement with equation (17). Ratios of 1 to 6 can be obtained for both low and high values of density and \mathcal{D} (or ζ_{esc}). In the first case from this ratio one can determine the parameters n and \mathcal{D} and in the latter case only the product $n\mathcal{T}_{esc}$.

This degeneracy can be broken from consideration of the spectral indices. Figures 9 show the variations of the photon number (not energy) spectral indices obtained from channels M1 and M2 (33-53 keV) for the foot point (left panel) and loop top (right panel) sources. As in Figure 8 the spectral index is plotted as a function of \mathcal{D} for three values of \mathcal{T}_{esc} (dashed, solid and dotted lines) and density n . The dotted horizontal lines show the observed values given in Table 2. The curves here decrease monotonically with \mathcal{D} and approach the asymptotic value of $\gamma = -d\ln J/d\ln k \rightarrow 1$ at high \mathcal{D} values, as expected from equation (12). The observations on the other hand favor values of \mathcal{D} in the lower range

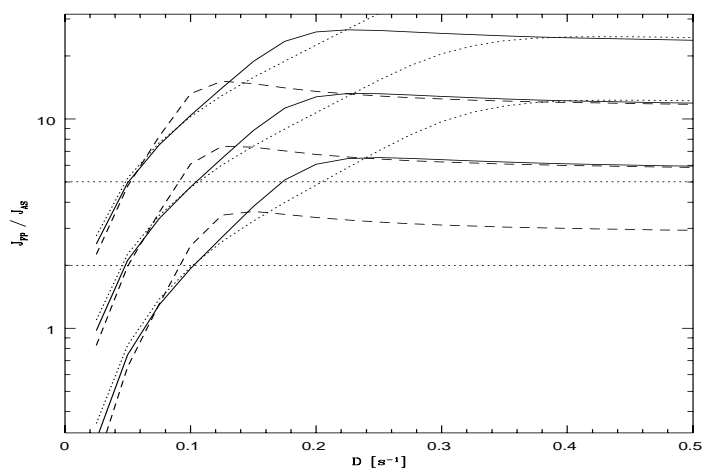


Fig. 8.— The ratio J_{FP}/J_{LT} in the 23 to 33 keV range (the M1 band) as a function of \mathcal{D} for three escape times $\mathcal{T}_{\text{esc}} = 0.05, 0.1$ and 0.2 s; dotted, solid and dashed lines, respectively, and for three values of density $n/(10^{10}\text{cm}^{-3}) = 2.5, 5$ and 10 ; in each case from top to bottom, respectively. The magnetic field $B = 300\text{G}$, $s = 1.5$ and $q' = 1.7$. The horizontal dotted lines show the range of the observed ratios.

($\mathcal{D} < 0.15 \text{ s}^{-1}$) and values for other parameters which are similar to the values obtained from the spectral fittings by PPS. These values are well within the acceptable ranges. For example, the January 13, 1992 flare with the ratio of 5 and spectral indices of 4.1 and 4.0 for the loop top and foot point sources, respectively, can be obtained with a model with $\mathcal{D} \simeq 0.08 \text{ s}^{-1}$, $\mathcal{T}_{\text{esc}} \simeq 0.05 \text{ s}$, $s = 1.5$, $q' = 1.7$ and $n \simeq 3 \times 10^{10} \text{ cm}^{-3}$, and for wide ranges for B and L . Similarly the October 4, 1992 flare with the ratio of about 4 and spectral indices of 5.2 and 3.4, respectively, can be fitted with almost same model parameters except $\mathcal{D} \simeq 0.09 \text{ s}^{-1}$, $\mathcal{T}_{\text{esc}} \simeq 0.07 \text{ s}$ and $n \geq 5 \times 10^{10} \text{ cm}^{-3}$. These values of \mathcal{D} , and the field strength of about 300G, require a turbulence energy density of $< 10^{-5} (B^2/8\pi)$ (cf, PPS).

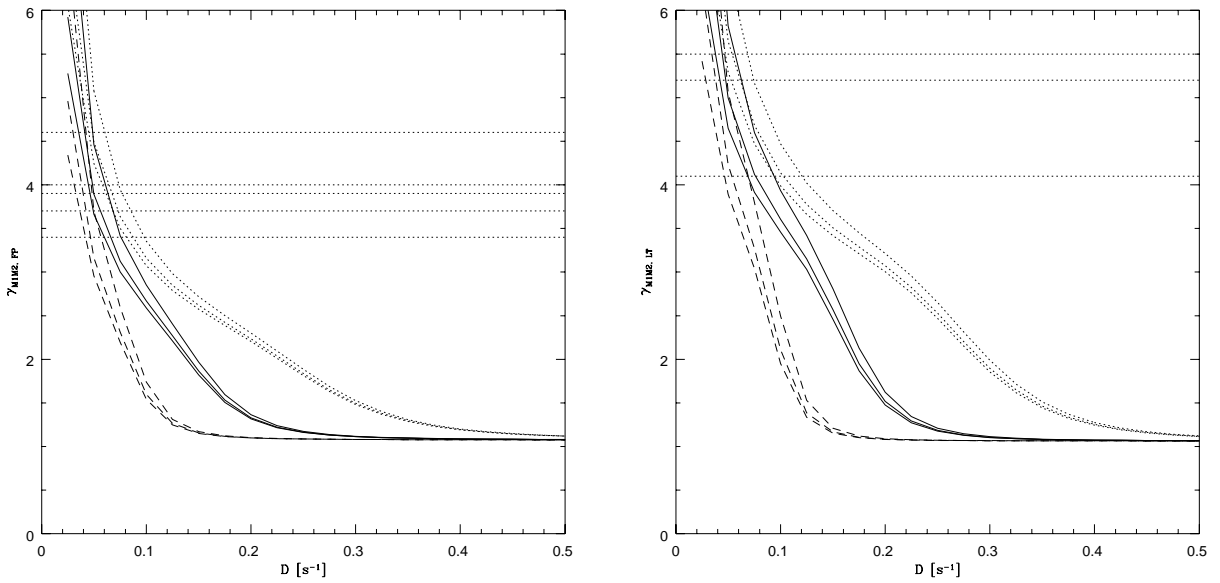


Fig. 9.— Same as Figure 8 but for the photon number spectral index ($\gamma = -d\ln J(k)/d\ln k$) between channels M1 and M2. Note that the order of the densities here is the opposite of that in Figure 8, increasing from bottom to top. The horizontal dotted lines show the observed values of this index given in Table 2. *Left Panel:* Foot point source *Right Panel:* Loop top source.

We repeat this analysis in Figure 10 for the whistler model. A wider range of behavior

is seen here because of the dependence of the \mathcal{T}_{esc} on the magnetic field, size and density (see, e.g. eq. [10] in PPS). Similar parameter values are obtained for the observed flares except in this case the magnetic field can be constrained to be greater than 100G.

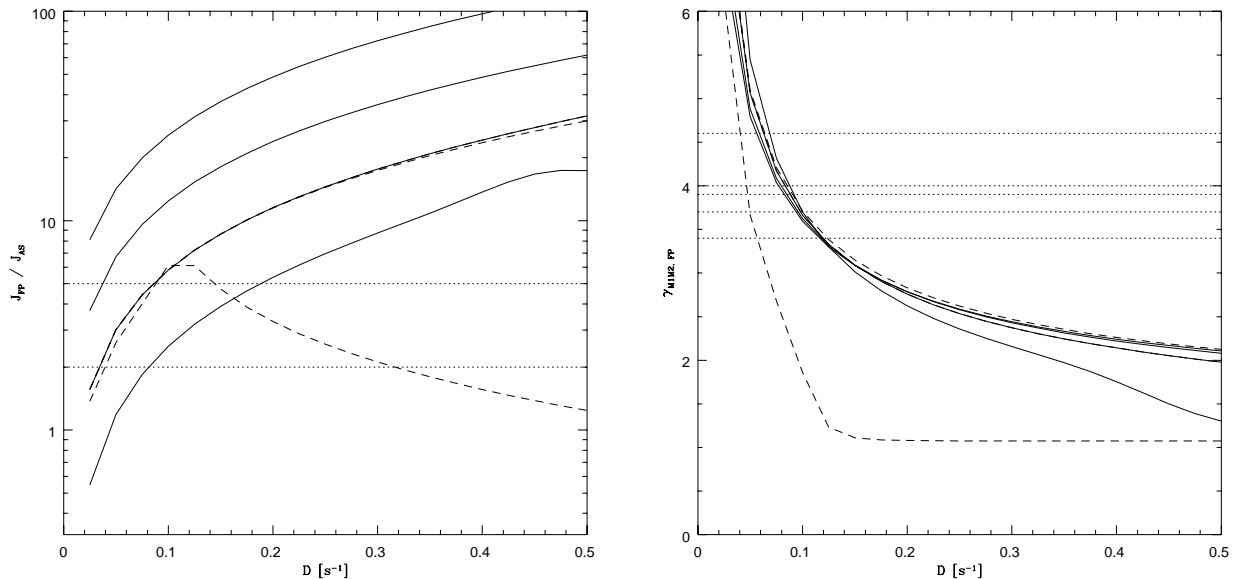


Fig. 10.— *Left Panel:* Same as Figure 8, except using the whistler wave acceleration model. The solid lines from top to bottom are for densities $n/(10^{10}\text{cm}^{-3}) = 1.25, 2.5, 5$ and 10 , respectively. $B = 300\text{G}$, $L = 10^9$ cm and $s = q' = 1.5$. The dashed lines show the effect of the magnetic field; $B = 1000\text{G}$, upper curve; $B = 100\text{G}$, lower curve. *Right Panel:* Variations of the photon number spectral index of the foot point source between channels M1 and M2 for the same model parameters as the left panel. Note that the increasing order of the density is for the high D end of the solid lines.

5. Summary and Discussion

In this paper we investigate the spatial structure of the impulsive phase hard X-ray emission. This work is motivated by the YOHKOH observations of hard X-rays from top of

flaring loops, presumably where particle acceleration takes place, as well as from their foot points, as is seen more commonly.

We first discuss the effects of particle transport in the usual thick target model whereby electrons are injected at the top of a flaring loop. We summarize the past results mainly from unpublished parts of J. Leach's (1984) thesis showing that a significant loop top emission, without any detectable emission from the legs of the loop, is possible in inhomogeneous loops where there is either a significant field convergence from the top to foot points or there is a strong density enhancement at the top of the loop. The former is a more natural expectation than the latter.

We point out two other possible explanations. The first is due to plasma turbulence at the acceleration site which can scatter and temporarily trap the electrons near the top of the loop giving rise to an enhanced emission as observed by YOHKOH. The second is if the accelerated particles have pancake type pitch angle distribution perpendicular to the field lines. Both of these could be a natural consequence of the stochastic acceleration model that has been investigated by Petrosian and colleagues (see e.g. Petrosian 1996 or PPS and references cited there) and Miller and colleagues (Miller et al. 1996 and Miller & Reames 1996).

A pancake type distribution can come about if acceleration is due to resonant scattering of electrons by plasma waves propagating perpendicular to the magnetic fields. As shown recently by Pryadko & Petrosian (1999) such interactions preferentially accelerate electrons with pitch angles near 90° . In this paper we have considered the more general case of stochastic acceleration that leads to an isotropic pitch angle distribution, in which case the loop top or acceleration site emission is a direct consequence of the scattering effects of the acceleration agent.

Following the formalism developed in PPS we evaluate separately the spectrum of

the radiation expected from the acceleration site and the foot points. We evaluate the relative strengths and spectral shapes of these two emissions and the dependence of these on the parameters describing the acceleration process and the flare plasma. The most important parameter is the product of the acceleration rate and the escape time; its value and energy dependence. We have adopted general parametric expressions for these quantities. In reality, as described by Pryadko & Petrosian (1997, 1998 and 1999) the determination of these parameters, which are obtained from the Fokker-Planck coefficients, is complicated and requires extensive numerical analysis. They depend strongly on the ratio of the plasma to gyro-frequency, or n/B^2 . The plasma density n and the field strength B also play important roles through their influence on the losses due to Coulomb collisions and synchrotron emission. The parametric forms chosen here are designed to mimic the behavior of the more accurate numerical results.

We first give a general description of the characteristics of these emissions and compare them with some approximate analytic expressions. We then compare the theoretical ratio of the intensities and spectral indices of the X-ray emissions with YOHKOH observations. We demonstrate how the above mentioned parameters can be constrained with such observations. The ranges of the parameters favored here is similar to those obtained through spectral fittings by PPS. The current spatially resolved information is not sufficient for setting strong constraints on the acceleration or flare plasma parameters or for distinguishing the stochastic acceleration model in general from other acceleration and transport models. Our purpose here has been to demonstrate the feasibility of this model and point out how future combined high spatial and spectral resolution data, for example those expected from HESSI, can answer these important questions.

Aside from using the simple parametric approximations mentioned above we have also used the assumption of pitch angle isotropy. At low energies this assumption may break

down. As shown by Pryadko & Petrosian (1997) for waves propagating along the magnetic field lines the acceleration time scale may become smaller than the scattering time and the latter may become longer than the traverse time $\tau_{tr} \sim L/v$. To account for this we have added the additional term to the escape time which is proportional to τ_{tr} . This does not fully take care of the problem arising with the possible anisotropy of the pitch angle distribution. Anisotropy can also arise in the presence of waves propagating perpendicular to the field lines because such waves accelerate electrons preferentially with pitch angles $\alpha \sim 90^\circ$ (Pryadko & Petrosian 1999). As mentioned above this can give rise to pancake type distribution which also can give rise to an enhanced emission near the acceleration site. The effects of these complications will be addressed in future publications.

This work is supported in parts by NASA grant NAG-5-7144-0002, Lockheed grant SA30G730R-AO7, and grants from Stanford's Undergraduate Research Opportunities and Bing Summer Science Fellowship Programs. TQD would like to thank Brian Park and Nicole Lloyd for helpful discussions on computational aspects of this work.

REFERENCES

- Alexander, D., & Metcalf, T. R. 1997, *ApJ*, 489, 442
- Bech, F.-W., Steinacker, J., & Schlickeiser, R. 1990, *Sol. Physics*, 129, 195
- Chandrasekhar, S. 1943, *Rev. Mod. Phys.*, 15, 1
- Dermer, C. D., & Ramaty, R. 1986, *ApJ*, 301, 962
- Dung, R., & Petrosian, V. 1994, *ApJ*, 421, 550
- Fletcher, L. 1995, *A&A (Letters)*, 303, L9
- Fletcher, L. 1996, *A&A* , 310, 661
- Fletcher, L., & Martens, P. C. H. 1998, *ApJ*, 505, 418
- Hamilton, R. J., & Petrosian, V. 1992, *ApJ*, 398, 350
- Holman, G. 1996, *BAAS*, 28, 939
- Koch, H. W., & Motz, J. W. 1959, *Rev. Mod. Phys.*, 31, 950
- Leach, J. 1984, Ph. D. Thesis, Stanford University
- Leach, J., & Petrosian, V. 1981, *ApJ*, 251, 781
- Leach, J., & Petrosian, V. 1983, *ApJ*, 269, 715
- Lu, E., & Petrosian, V. 1989, *ApJ*, 338, 1122
- Masuda, S. 1994, Ph.D. Thesis, The University of Tokyo
- Masuda, S. et al. 1994, *Nature*, 371, 455

- Marsh, K. A., & Hurford, G. J. 1980 ApJ (Letters), 240, L111
- McTiernan, J. M., & Petrosian, V. 1990a, ApJ, 359, 524
- McTiernan, J. M., & Petrosian, V. 1990b, ApJ, 359, 541
- McTiernan, J. M., & Petrosian, V. 1991, ApJ, 379, 381
- Miller J.A. 1991, ApJ. 376, 342
- Miller, J. A., LaRosa, T. N., & Moore, R. L. 1996, ApJ, 445, 464
- Miller, J. A., & Rreams, D. V. 1996, in High Energy Solar Physics, eds. R. Ramaty, N. Mandzhavidze & X-M. Hua (AIP Conf. Proc. 374), 450
- Park, B. T., & Petrosian, V. 1995, ApJ, 446, 699
- Park, B. T., & Petrosian, V. 1996, ApJS, 103, 255
- Park, B. T., Petrosian, V., & Schwartz, R. A. 1997, ApJ, 489, 358 (**PPS**)
- Petrosian, V. 1973, ApJ, 186, 291
- Petrosian, V. 1982, ApJ (Letters), 255, L85
- Petrosian, V. 1994, in High-energy Solar Phenomena, eds. J. M. Ryan & W. T. Vestrand (AIP Conf. Proc. 294), 162
- Petrosian, V. 1996, in High Energy Solar Physics, eds. R. Ramaty, N. Mandzhavidze & X-M. Hua (AIP Conf. Proc. 374), 445
- Petrosian, V., McTiernan, J. M., & Marschhäuser, H. 1994, ApJ, 434, 747
- Pryadko, J., & Petrosian, V. 1997, ApJ, 482, 774
- Pryadko, J., & Petrosian, V. 1998, ApJ, 495, 377

Pryadko, J., & Petrosian, V. 1999, ApJ, 515, in press

Ramaty, R. 1979, in Particle Acceleration Mechanisms in Astrophysics, eds. J. Arons, C. Max & C. McKee (AIP conf. proc., No. 56), 135

Ramaty, R., & Murphy, R. J. 1987, Space Sci. Rev., 45, 213

Schlickeiser, R. 1989, ApJ, 336, 243

Wheatland, M. S., & Melrose, D. B. 1995, Sol. Physics, 185, 283